




Article

Photocatalytic Activity in the In-Flow Degradation of NO on Porous TiO₂-Coated Glasses from Hybrid Inorganic–Organic Thin Films Prepared by a Combined ALD/MLD Deposition Strategy

Ramón Azpiroz ¹, Marina Borraz ², Aida González ^{1,3}, Catalina Mansilla ^{2,*}, Manuel Iglesias ^{1,*} and Jesús J. Pérez-Torrente ^{1,*}

¹ Departamento de Química Inorgánica, Instituto de Síntesis Química y Catálisis Homogénea-ISQCH, Universidad de Zaragoza-C.S.I.C., 50009 Zaragoza, Spain; rayazp2@gmail.com (R.A.); a.gonzalez@duglass.es (A.G.)

² Ctechnano, Av. de Tolosa 76, 20018 San Sebastian, Spain; m.borraz@ctechnano.com

³ Ariño Duglass, Pol. Ind. Royales Bajos s/n, Puebla de Alfindén (Ia), 50171 Zaragoza, Spain

* Correspondence: c.mansilla@ctechnano.com (C.M.); miglesia@unizar.es (M.I.); perez@unizar.es (J.J.P.-T.)

Abstract: A combined ALD/MLD (where ALD and MLD stand for atomic and molecular layer deposition, respectively) deposition strategy using TiCl₄, H₂O and HQ (hydroquinone) as precursors has been applied for the preparation of inorganic–organic thin films on soda-lime glasses. The alternate deposition of TiO₂ layers, by pulsing TiCl₄/H₂O (ALD), and hybrid layers, using TiCl₄/HQ (MLD), results in the formation of thin films that are precursors for porous TiO₂-coatings after removal of the HQ template by annealing. The coated-glasses show good photocatalytic activity in the degradation of NO with up to 15% reduction of NO concentration in three successive photocatalytic cycles of 5 h each. Surface Scanning Electron Microscopy (SEM) images show that the TiO₂-coating is composed of large grains that are made up of finer subgrains resulting in a porous structure with an average pore size of 3–4 nm. Transmission Electron Microscopy (TEM) images show two regions, a porous columnar structure on top and a denser region over the glass substrate. Energy Dispersive X-Ray (EDX) analysis, nanocrystal electron diffraction and Raman spectroscopy confirm the presence of the anatase phase, which, together with the porosity of the material, accounts for the observed photocatalytic activity.

Keywords: hybrid inorganic-organic; molecular layer deposition (MLD); atomic layer deposition (ALD); titanium dioxide; anatase; nitrogen monoxide; photocatalysis



Citation: Azpiroz, R.; Borraz, M.; González, A.; Mansilla, C.; Iglesias, M.; Pérez-Torrente, J.J. Photocatalytic Activity in the In-Flow Degradation of NO on Porous TiO₂-Coated Glasses from Hybrid Inorganic–Organic Thin Films Prepared by a Combined ALD/MLD Deposition Strategy. *Coatings* **2022**, *12*, 488. <https://doi.org/10.3390/coatings12040488>

Academic Editor: Joaquim Carneiro

Received: 1 March 2022

Accepted: 1 April 2022

Published: 5 April 2022

Publisher's Note: MDPI stays neutral with regard to jurisdictional claims in published maps and institutional affiliations.



Copyright: © 2022 by the authors. Licensee MDPI, Basel, Switzerland. This article is an open access article distributed under the terms and conditions of the Creative Commons Attribution (CC BY) license (<https://creativecommons.org/licenses/by/4.0/>).

1. Introduction

The combustion of fossil fuels in mobile and stationary power sources results in the generation of nitrogen oxides (NO_x), which are key contributors to the photochemical smog and air pollution in urban areas. Photochemical smog consists mainly of tropospheric ozone (O₃), peroxyacyl nitrates (PANs), particulate matter (PM), and nitric acid. The latter is formed by the reaction of NO₂ with water, whilst the generation of radicals by the interaction of NO_x and sunlight is, to a great extent, the origin of O₃, PANs and PM. The environmental and health related problems associated with the emissions of NO_x's are diverse, and include (i) acidic depositions, which are harmful to aquatic life, crops and forests, (ii) and adverse effects on human health, which primarily affect the respiratory and cardiovascular systems. In this context, the development of systems that reduce the concentration of NO_x's in the atmosphere is of paramount importance to improve the quality of life in major cities [1–3].

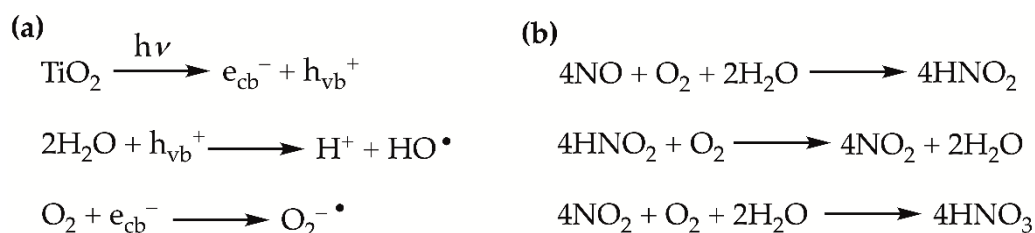
Titanium dioxide (TiO₂) is a prolific semiconductor photocatalyst [4–8] that has shown activity in the degradation of NO_x's via UV irradiation, since the band-gap of these materi-

als usually ranges approximately from 3.0 to 3.2 eV. Longer wavelength absorption has been achieved by doping with nitrogen and transition metals, which allows the photocatalyst to work under visible light irradiation [9].

TiO₂ exists in nature in three crystalline phases; namely, anatase, rutile and brookite [10–12]. Rutile is the most thermodynamically stable phase, while anatase and brookite are metastable and, therefore, may be converted irreversibly into the rutile phase at high temperatures [13–17]. However, it must be noted that the relative stability of the different TiO₂ phases depends on the particle size, degree of agglomeration, and the nature of the support [17–21]. The physical and chemical properties of TiO₂ depend on the structural parameters of each polymorph, which determines the photocatalytic activity of the material. TiO₂-anatase shows better catalytic performance than TiO₂-rutile due to (i) its higher electron mobility [22], (ii) greater number of active sites (oxygen vacancies), and (iii) the broader band-gap of anatase (3.20 eV for anatase and 3.02 eV for rutile), which results in a slightly superior redox capability [23]. The photocatalytic activity of TiO₂-anatase may be improved by increasing the porosity of the material [24]. This porosity may be achieved by supporting the TiO₂ on intrinsically porous surfaces, such as, zeolites, inverse opal-like structures, tiles, ceramics or asphalt pavement [8,25–28] or by the preparation of porous TiO₂ materials [29–39]. The molecular layer deposition (MLD) technique is a variation of ALD (atomic layer deposition) that makes use of molecular organic and inorganic precursors, thus allowing for the formation of molecular layers or the preparation of hybrid inorganic-organic films. The use of TiCl₄ and bifunctional organic reactants (e.g., ethylene glycol, glycerol or hydroquinone) as precursors has been reported as a suitable method for the preparation of titanocene thin-films upon annealing [38,39]. The deposition of successive layers of TiCl₄ and organic spacers by means of multiple MLD cycles leads to the formation of an inorganic-organic film. Subsequently, thermal annealing causes the combustion and removal of the organic spacers, thus creating cavities in the structure that eventually result in the formation of a porous-TiO₂ material [39–42]. This apparently simple methodology, however, presents shortcomings and drawbacks regarding the size of the spacer and the conditions employed for the thermal annealing. The former involves the difficult vaporization of large molecules under MLD conditions, which limits the pore size. The latter is caused by the fact that high temperatures and long annealing times are required for the formation of anatase from amorphous TiO₂, but the collapse of the porous structure, and even anatase-to-rutile phase transformation, may occur under these conditions [43]. Therefore, fine-tuning of MLD and annealing conditions is key to achieving appropriate porosity and anatase proportions able to induce photocatalytic activity.

The activity of TiO₂-materials deposited by MLD has been investigated employing benchmark test reactions such as the photodegradation of methylene blue [43–45], Azure B [46] or porphyrin [39]. However, to the best of our knowledge, in contrast with TiO₂ coatings deposited by other techniques [47], the photodegradation of nitrogen oxides remains unexplored for TiO₂ films generated by MLD processes.

The photocatalytic removal of nitric oxide (NO) employing functionalized ceramic materials is regulated by the ISO 22197-1:2007 [48], thus providing a standardized methodology to test the photocatalytic activity of different coatings and substrates. In the case of TiO₂ surfaces, the oxidation of NO under UV-irradiation entails the set of reactions depicted in Scheme 1. The irradiation of TiO₂ with UV-light (<387 nm) triggers the creation of electron (e⁻)/hole (h⁺) pairs as electrons are excited from the valence to the conduction band. H₂O molecules or OH⁻ ions adsorbed on the TiO₂ surface react with the holes, while adsorbed O₂ is reduced by an electron. These reactions afford hydroxyl (OH•) and superoxide (O₂^{-•}) radicals, which are responsible for the oxidation of NO_x's. Ultimately, the oxidation of NO_x's leads to the formation of HNO₃ and NO₃⁻ on the TiO₂ surface (Scheme 1) [49]. The build-up of these species on the TiO₂ surface deactivates the photocatalyst, which is re-activated by rinsing the surface with water [50].



Scheme 1. (a) Generation of hydroxyl and superoxide radicals. (b) Overall photocatalytic reactions for the oxidation of NO on a TiO₂ surface.

We report herein on the preparation of glasses coated with a thin film of porous anatase deposited by ALD/MLD and the evaluation of their photocatalytic activity in the in-flow degradation of NO(g). In this regard, we have followed two different approaches: (i) MLD deposition of titanicon thin films, and (ii) ALD/MLD deposition of hybrid inorganic-organic superlattice thin films. The presence of porous anatase in the photocatalytic coatings has been confirmed by Raman spectroscopy, X-ray diffraction (XRD) and electron microscopy techniques.

2. Materials and Methods

The studies were carried out on flat soda-lime glasses of 100 mm × 50 mm × 6 mm (height, width and thickness) manufactured by Guardian coated with a 10 nm thin film of SiO₂ deposited by PVD (Physical Vapor Deposition-Magnetron Sputtering) at the Department of Applied Physics of the University of Zaragoza [51]. Previously, the glasses were washed with water and soap and dried on an absorbent paper. The SiO₂ coating plays a multifaceted role, as it inhibits the diffusion of alkaline ions from the glass substrate to the photocatalytic coating during the annealing process [45,52], provides thermal stability to the supported TiO₂ via the formation of covalent Ti–O–Si bonds [22], while it prevents agglomeration, phase transformation and assist the adsorption process, increasing optical path length [53].

The ALD/MLD depositions were carried out in a PLAY Series Tool (CTECHnano, Coating Technologies S.L, San Sebastián, Spain) using nitrogen (N₂) as a carrier gas for the precursors and as a purging gas. Flat soda-lime glasses with 10 nm of SiO₂ deposited by sputtering and silicon wafers were used as substrates. Titanicon films [38] (labeled as Titanicon EG) were deposited using titanium tetrachloride (TiCl₄; Honeywell Fluka ≥ 99.0%, Madrid, Spain) and ethylene glycol (EG; Sigma-Aldrich 99.8%, St. Louis, MO, USA) as precursors according to the following pulse sequence TiCl₄ (0.3 s)/15 s/N₂ (60 s)/EG (1 s, 70 °C)/15 s/N₂ (90 s), 200 cycles, with a deposition temperature of 110 °C. Other Titanicon (Ti–O–C₆H₄–O)_k thin films (labeled as Titanicon HQ) were deposited using TiCl₄ and hydroquinone (HQ; Sigma-Aldrich ≥ 99.5%) as precursors, with a sequence per cycle as: TiCl₄ (0.2 s)/N₂ (60 s)/HQ (12 s)/N₂ (70 s).

Hybrid [(TiO₂)_m(Ti–O–C₆H₄–O)_k]₁₂₀ superlattice was deposited using TiCl₄ and HQ as a precursors and deionized water (H₂O) as a co-reactant, by mixing the deposition process for Titanicon HQ films with the TiCl₄/H₂O ALD process for TiO₂ [54]. To deposit an ALD cycle of TiO₂, the precursors were pulsed in the following manner: TiCl₄ (0.2 s)/N₂ (60 s)/H₂O (0.2 s)/N₂ (65 s). To reach the precursor vapor pressures required for efficient precursor transport to the substrate, HQ was heated up to 120 °C, whereas TiCl₄ and H₂O were kept at room temperature. The deposition temperature was set at 210 °C for all of the experiments. Two different structures were prepared. The first one consisted in 20 cycles of TiCl₄/H₂O following by 500 cycles of TiCl₄/HQ. The second one was prepared by mixing *m* cycles of TiCl₄/H₂O, with then *k* cycles of TiCl₄/HQ, and repeated the process 120 times in order to fabricate thin films with superlattice structures. Hence, different *k*:*m* ratio was effectively used to control the superlattice period, the total number of deposition cycles was obtained as (*m* + *k*) × 120. After the deposition process, samples were subjected to thermal annealing in a UNITEMP RSO-200 series furnace (UniTemp, Pfaffenhofen; Germany). The

optimized treatment was an instantaneous temperature rise to 250 °C, a temperature ramp to 450 °C in 90 min (2.2 °C/min), and finally 3 h at that temperature.

Film thicknesses were determined by means of X-ray reflectivity (XRR) in a X'Pert PRO PANalytical X-ray diffractometer (Malvern Panalytical, Malvern, UK). Scanning Electron Microscopy (SEM) and High-Resolution Transmission Electron Microscopy (HRTEM) images of the coated-glasses were obtained using eSEM-FEI Quanta™ 250 (and FEI Titan 80-300 TEM microscopes (Fei Company, Hillsboro, USA), respectively, at the Structural-Morphology Characterization Service of CIC NanoGUNE. A thin sample for TEM was prepared using dualbeam instrument FEI Helios 450 with standard lift out and thinning protocols [55]. Raman and UV-Vis spectra were performed at the Chromatography and Spectroscopy Service of the ISQCH. Raman spectra were recorded on a JASCO NRS 3100 spectrophotometer (JASCO, Tokyo, Japan), equipped with a high performance 532 nm laser, and are the result of subtracting the glass signal to the Raman spectra obtained from the coated-glasses. UV-Vis spectra were recorded directly on coated-glass samples on a JASCO V-670 dual beam spectrophotometer (JASCO, Tokyo, Japan), using clean uncovered glass as reference sample. Bandgaps were determined by Tauc plot method [56] using the bandgap calculation subroutine embedded in Jasco Spectra Analysis software (version 1.0). X-ray diffraction measurements were carried out at the X-ray Diffraction and Fluorescence Analysis Service of the Servicio General de Apoyo a la Investigación-SAI, Universidad de Zaragoza. XRD patterns were recorded on a RIGAKU diffractometer (Rigaku Corporation, Tokyo, Japan), model Ru2500, equipped with a rotating Cu anode. The diffractometer operates at 40Kv and 80 mA using a graphite monochromator to select the CuK α radiation. Data were collected in a 2 θ range of 20–60°, step = 0.03°, t = 3 s/step.

The photocatalytic activity of the coated-glasses was measured in an inert flat-bed photoreactor designed and manufactured by the company Ariño Duglass according to ISO 22197- 1:2007 [48]. The experimental setup including the gas supply, photoreactor, and analytical system is shown in Figure 1. The photoreactor consists of a stainless-steel reaction chamber designed to hold 50 cm² glass samples (50 mm × 100 mm) of variable thicknesses on Teflon holders equipped with a borosilicate glass window. The irradiation source was a 36 W black light (Philips Actinic BL TL-DK; the wavelengths emitted range from 340 to 400 nm with a maximum at 370 nm) placed over the reactor at 6.5 cm from the sample with an irradiance (incident power/area) of 10 W/m². The reactor is fed with a NO/N₂ certified mixture as polluting gas (120 ppm of NO(g), Nippon Gases) and high purity synthetic air (Nippon Gases). A stream of air was bubbled through a gas wash bottle containing water to control the humidity. The dry air, moist air and N₂/NO streams were regulated with mass flow controllers (Bronkhorst, F-201CV) and mixed to obtain the desired NO(g) concentration. The system is equipped with a stainless-steel static gas mixer (Koflo Pipe Mixer) before reactor inlet, and temperature and humidity sensors at the reactor inlet and outlet. The gas flows were: 1.50 and 1.47 L/min for dry and wet synthetic air, respectively, and 30 mL/min for the N₂/NO polluting gas. After a stabilization period, the concentration of NO(g) through the reactor was 1 ± 0.05 ppm with a flow rate of 3 L/min. Note that the stabilization period is the time required to reach a stable concentration of 1 ± 0.05 ppm of NO and a humidity of 50%, since the flows of NO, dry synthetic air and wet synthetic air need to mix correctly before the start of the experiment. NO(g) and NO₂(g) concentrations in the outlet gas stream from the reactor were continuously monitored by using electrochemical gas sensors (Alphasense Ltd., Braintree, UK, NO-A4 and NO₂-A4F3). The concentration of both gases, temperature and humidity data were recorded in a computer by using software designed by the Electronic Instrumentation Service (SAI) from the University of Zaragoza for this purpose. The outlet gas stream is bubbled through a gas wash bottle containing a concentrated NaOH solution.

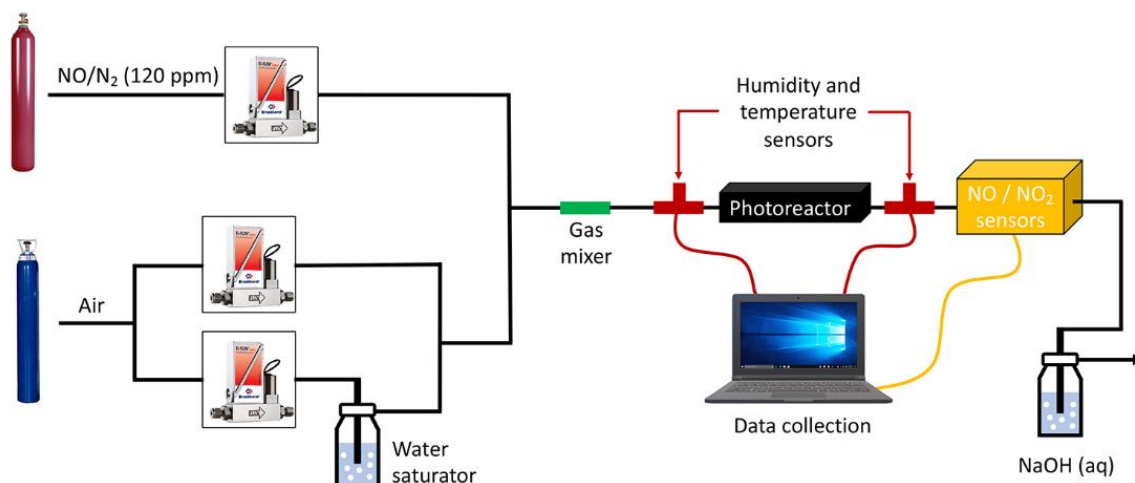


Figure 1. Schematic representation of the experimental setup.

The photocatalytic tests were performed at room temperature with a relative humidity of 50% at 25 °C. The measurements were carried out continuously for 4–5 h with a data collection every 7 s. At the end of the measurement, the coated-glasses were washed with distilled water in order to determine the NO₂[−] and NO₃[−] concentration using a colorimetric indicator from Hasch. A test strip was dipped into the solution obtained by washing the surface with distilled water (≈2 mL) after the photocatalytic experiments. Positive tests result in a color change which is compared with the chart provided by the manufacturer for the semi-quantitative determination.

Coated-glasses with significant photocatalytic activity were washed with Milli-Q water, dried on an absorbent paper and subjected to successive photocatalytic cycles every 24 h under the same conditions.

3. Results

3.1. MLD of Titanicone EG Thin Films on Glass as Precursors for Photocatalytic Coatings

Titanicone EG thin films on glass were prepared according to the literature procedure [57]. The hybrid inorganic-organic coatings based on titanium-alkoxide were deposited using TiCl₄ and ethylene glycol (EG), a relatively low boiling point diol, as precursors using a standard pulse sequence (see above). In parallel, the deposition was performed on silicon wafers (1 cm × 1 cm) to determine the thickness of the coating by X-ray reflectometry (XRR). Under these conditions, the measured film thickness after 200 cycles was about 90 nm, which corresponds to a growth per cycle value (GPC) of 0.45 nm/cycle. Finally, annealing at 400 °C for 2 h in air to remove the organic template and transform the amorphous TiO₂ into the anatase crystalline phase resulted in a uniform and transparent coated-glass. The coating thickness was reduced to 30 nm after the thermal treatment, which agrees with the elimination of the organic groups connecting the different titanium centers in the hybrid material.

The photocatalytic activity of this coated-glass in the degradation of NO(g) is shown in Figure 2a. As can be seen, the NO(g) concentration is slightly reduced, by 0.04 ppm, once the illumination is turned on and it is maintained over the 4 h of the experiment until the illumination is turned off (NO₂(g) formation was not observed). SEM analysis of surface morphology showed no evidence of porosity suggesting a microporous structure with a pore size of less than 2 nm (Figure S22). The coating thickness determined by the cross-sectional image was approximately 20 nm, which is of the same order of magnitude as that determined by XRR (30 nm). The Raman spectrum showed three strong characteristic bands at 639, 513, and 399 cm^{−1} corresponding to the anatase phase, which is consistent with the observed photocatalytic activity. Interestingly, no Raman bands for the rutile phase were observed. In contrast, a coated-glass with TiO₂ using TiCl₄ and H₂O as precursors

under similar ALD conditions and annealed at 400 °C for 3 h showed no photocatalytic activity, highlighting the positive influence of EG on the coating properties (Figures S16 and S17).

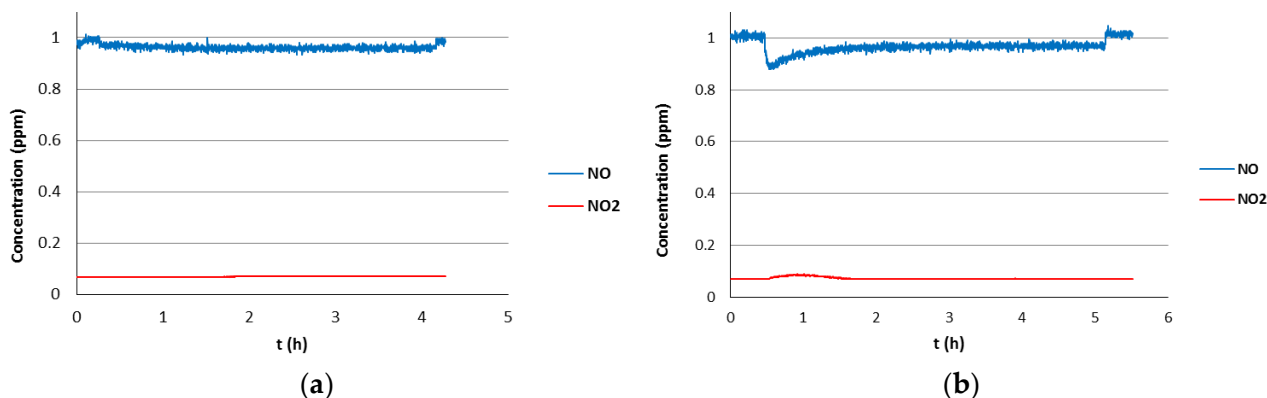


Figure 2. Photocatalytic activity in the degradation of NO(g) of coated-glasses fabricated from MLD Titanicone EG thin films (TiCl_4/EG) after thermal treatment. (a) EG (1 s, 70 °C), thermal treatment: annealing at 400 °C for 2 h. (b) EG (4 s, 80 °C), thermal treatment: RT to 250 °C (1 min), 250 to 400 °C (90 min), 3 h at 450 °C (optimized annealing conditions).

The influence of the thermal treatment on the photocatalytic activity of the coated-glasses has been investigated as well. Thus, an inorganic-organic film deposited on glass by MLD under the same conditions as described above was subjected to a different annealing program. First, an instantaneous temperature rise to 250 °C was applied, a temperature ramp to 450 °C in 90 min (2.2 °C/min), and finally 3 h at that temperature. The resulting coated-glass showed a slightly higher photocatalytic activity than the glass treated at 400 °C, with a reduction of the NO(g) concentration of 0.05 ppm over 4 h (Figure S2). The slight improvement in the photocatalytic activity prompted us to apply these conditions in the following experiments (optimized annealing conditions).

The limited photocatalytic activity of the samples evaluated in Figure 2 is probably a consequence of the lack of porosity. To find the best conditions to prepare porous TiO_2 anatase thin films on glass by MLD, we have investigated the influence of increasing: (i) the EG temperature from 70 to 80 °C, (ii) the EG pulse time from 1 to 1.5 s, (iii) the maximum temperature of the heating ramp from 450 to 550 °C during annealing, and (iv) the time at the maximum temperature during annealing (450 °C) for 5 h (Tables S2–S6). Unfortunately, no significant increase in photocatalytic activity was observed in any case. Nevertheless, increasing the EG pulse time to 1.5 s produces a slight improvement of the photocatalytic activity at the beginning of the experiment although after 2 h the average reduction of the NO(g) concentration is 0.04 ppm, identical to that observed with a time of 1.0 s. On the other hand, increasing the maximum temperature to 550 °C or prolonged heating showed a negative effect. This activity drop is likely due to the collapse of the porous structure, which is pivotal to achieve catalytic activity in the photodegradation of NO, although anatase-to-rutile phase transformation cannot be discarded.

Finally, two coated-glasses have been prepared in an attempt to maximize the EG transfer to the substrate. In the first one, the EG pulse time was increased to 4.0 s, and in the second, two consecutive EG pulses of 4.0 s each were programmed, keeping in both cases identical deposition conditions (EG temperature of 80 °C) and the optimized annealing treatment. The first of the coated-glass showed an initial decrease in NO(g) concentration to 0.89 ppm and $\text{NO}_2(\text{g})$ formation of 0.02 ppm, although the photocatalytic activity decays with time and stabilizes at 0.97 ppm of NO(g) after 2 h (Figure 2b). The second coated-glass showed no photocatalytic activity, which may be due to the fact that the addition of two consecutive EG pulses results in a fragile structure that collapses during the annealing process.

3.2. Photocatalytic Coatings on Glass from Hybrid Inorganic–Organic Superlattice Thin Films

Klepper and co-workers have described the preparation of alucones, inorganic–organic hybrid films based on trimethylaluminum (TMA). A range of aromatic and aliphatic dicarboxylic acids have been used for the preparation of alucone coatings on soda-lime glass and silicon single crystals [57,58]. However, hybrid inorganic–organic thin films prepared by MLD using TiCl_4 and terephthalic acid (benzene-1,4-dicarboxylic acid) under different deposition conditions resulted, after the optimized annealing treatment, in coated-glasses that showed no photocatalytic activity in the degradation of $\text{NO}(\text{g})$.

Recently, Knez and co-workers have described the preparation of alucones using hydroquinone (HQ) as an organic template [59]. Therefore, the preparation of inorganic–organic hybrid coatings using TiCl_4 and hydroquinone (HQ) could be possible. However, the small size and rigidity of HQ likely limits its ability to induce porosity. Therefore, we decided to follow the methodology reported by Karppien and co-workers [54], who developed a combined ALD/MLD deposition strategy to prepare inorganic–organic thin films using TiCl_4 , H_2O and HQ as precursors. Thus, the combination of hybrid ($\text{Ti}-\text{O}-\text{C}_6\text{H}_4-\text{O}-$) layers prepared, by TiCl_4/HQ MLD, with TiO_2 layers, prepared by $\text{TiCl}_4/\text{H}_2\text{O}$ ALD, results in the formation of $[(\text{TiO}_2)_m(\text{Ti}-\text{O}-\text{C}_6\text{H}_4-\text{O}-)_k]_n$ coatings which are composed by layers of amorphous TiO_2 linked to HQ (Figure 3). Thermal annealing should result in the formation of a porous TiO_2 anatase coating after removal of the HQ template.

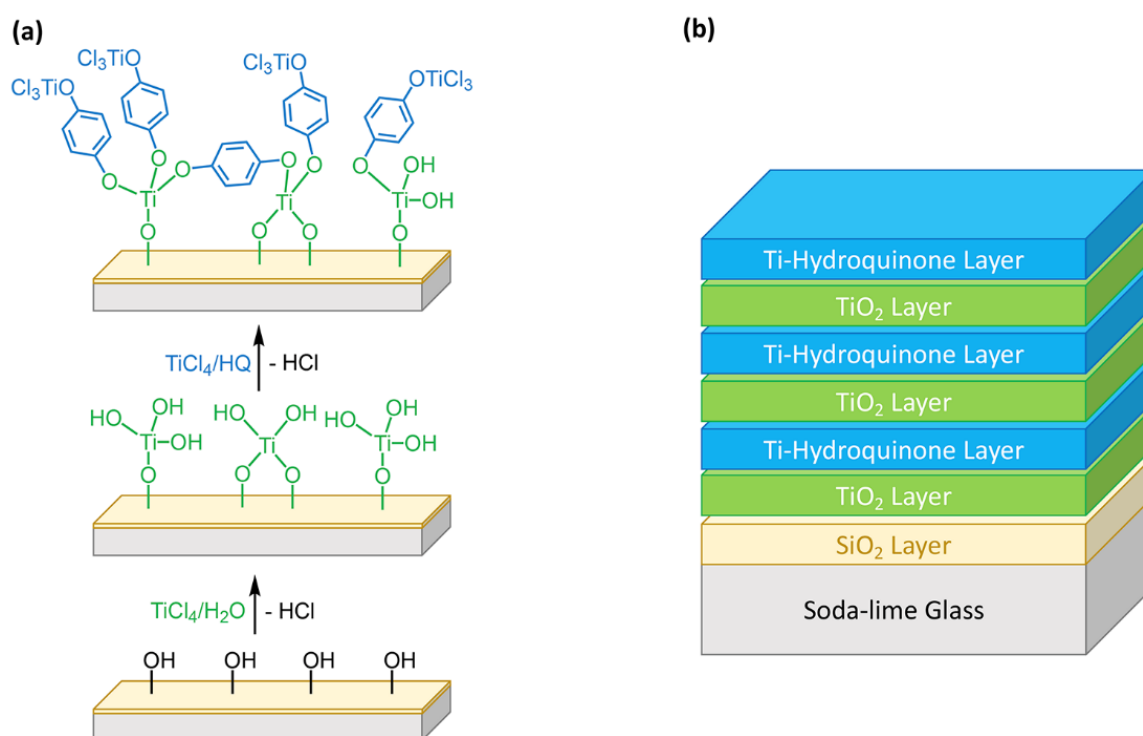


Figure 3. Schematic representation for the deposition of inorganic–organic thin films on glass composed of TiO_2 layers (prepared by $\text{TiCl}_4/\text{H}_2\text{O}$ ALD) and hybrid Ti/HQ layers (prepared by TiCl_4/HQ MLD): (a) sequential deposition of single cycle ALD/MLD layers; (b) sequential deposition of TiO_2 and Ti-HQ layers generated by multiple ALD and MLD cycles, respectively [58].

The first coating was prepared in two steps. Initially, TiCl_4 and H_2O were pulsed under the specified conditions (20 cycles) to deposit a TiO_2 layer. Subsequently, a monolayer of the hybrid film was deposited using TiCl_4 and HQ (500 cycles) (Figure 3a). The resulting coating has a thickness of 84 nm, which was reduced to about 30 nm (XRR) after the optimized annealing treatment. The obtained coated-glass is transparent and shows a uniform coating. However, the glass showed virtually no photocatalytic activity, i.e., no significant decrease of the NO concentration has been observed under irradiation (Figure S10).

In view of this result, it was decided to explore a more homogeneous alternating deposition sequence. First, $\text{TiCl}_4/\text{H}_2\text{O}$ were used as precursors (2 cycles) and subsequently TiCl_4/HQ (4 cycles), repeating this sequence 120 times following the deposition conditions described in Section 2 (Figure 3b). The coated-glass obtained after the optimized annealing treatment is also transparent and shows a uniform coating over the entire surface. However, in contrast with the previous sample, the film thickness after the thermal treatment increases from 25 to 46 nm (XRR), which could be indicative of increased porosity induction. The transparent coated-glass fabricated under these conditions showed photocatalytic activity. As can be seen in Figure 4a, initially there is a decrease in $\text{NO}(\text{g})$ concentration to 0.75 ppm and $\text{NO}_2(\text{g})$ formation to 0.07 ppm and then, the photocatalytic activity steadily stabilizes at 0.90 ppm of $\text{NO}(\text{g})$ and 0.04 ppm of $\text{NO}_2(\text{g})$ over the remaining 4 h of experiment. The coated-glass was subjected to successive photocatalytic cycles by washing several times with distilled water and dried on absorbent paper after each cycle. Although the photocatalytic activity is maintained in the second photocatalytic cycle, a slight decrease was observed in the third cycle (Figure S11). Interestingly, analysis of the washings with test strips showed the presence of NO_2^- and NO_3^- which is consistent with the observed photocatalytic activity.

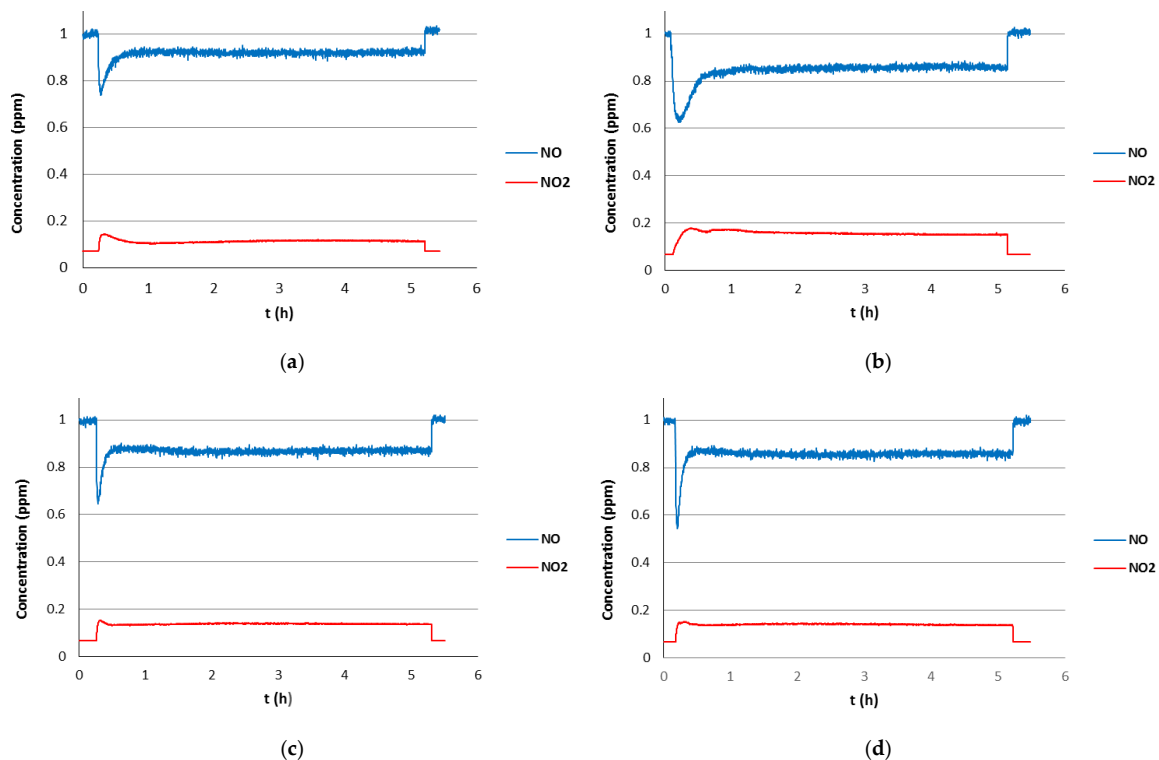


Figure 4. Photocatalytic activity in the degradation of $\text{NO}(\text{g})$ of coated-glasses formed by alternating inorganic (TiO_2) and inorganic-organic (TiCl_4/HQ) layers after optimized thermal treatment: (a) layers deposited at 2/4 ratio (120 cycles), (b) layers deposited at 2/8 ratio (120 cycles). Photocatalytic activity of the last coated-glass in the second (c) and third photocatalytic cycle (d).

After this successful experiment we decided to explore a similar alternating deposition sequence increasing the frequency of the TiCl_4/HQ pulses. Thus, alternate layers of inorganic (TiO_2) and hybrid (Ti/HQ) films have been deposited using $\text{TiCl}_4/\text{H}_2\text{O}$ (2 cycles) and TiCl_4/HQ (8 cycles) as precursors, repeating this sequence 120 times, under the conditions specified above. The coated-glass fabricated after annealing under optimized conditions showed higher photocatalytic activity. Initially, the amount of $\text{NO}(\text{g})$ decreases to 0.64 ppm and stabilizes at 0.85 ppm $\text{NO}(\text{g})$ and 0.08 ppm $\text{NO}_2(\text{g})$ along the experiment (Figure 4b). The pronounced decrease in $\text{NO}(\text{g})$ concentration at the beginning of the

experiment compared to the previous glass is a diagnostic of increased coating porosity which is consistent with the improved photocatalytic activity. It should be noted that this coated-glass showed stable photocatalytic behavior, since the activity is preserved in successive photocatalytic cycles. Thus, the NO(g) concentration stabilizes at 0.87 ppm with NO₂(g) formation of 0.07 ppm along the second and third photocatalytic cycles (Figure 4c,d). This coated-glass is iridescent with two zones with different light behavior, one violet and the other bluish. The Raman spectra of both zones are very similar showing the presence of anatase, bands at 639, 513, and 399 cm⁻¹. However, the intensity of the Raman bands is different, suggesting that this effect could be a consequence of the difference in thickness of the coating. In addition, the presence of the anatase TiO₂ phase was also confirmed by the XRD diffraction pattern (Figure S20).

Finally, we explored the effect of increasing the frequency of the TiCl₄/H₂O pulses. A deposition sequence of TiCl₄/H₂O (4 cycles) and TiCl₄/HQ (2 cycles) was applied and repeated 120 times. The coated-glass prepared under these conditions showed very little photocatalytic activity with a NO(g) concentration stabilization value of 0.98 ppm throughout the experiment. Therefore, decreasing the relative amount of HQ has a negative impact on the photocatalytic activity, which confirms the key role played by hydroquinone in the generation of porous structures.

SEM and TEM images of the coated-glass exhibiting best photocatalytic performance (Figure 4b) are shown in Figure 5 and in Figures S23–S25 and S27. Surface SEM images show that the film is composed of grains (≈30–150 nm) (Figure 5a) which are built of finer subgrains resulting in a porous structure with an average pore size of 3–4 nm (min. 0.8 nm, max. 13 nm). Low magnification cross-sectional TEM images show a film thickness of about ≈ 180 nm and evidence a columnar structure with the grains elongated along the thickness of the film. TEM images at higher magnification reveal two distinct regions in the film: a dense zone (≈45 nm) was observed at the bottom (near the substrate) and a highly porous zone at the top (≈125 nm). A thin layer of protective SiO₂ (≈10nm) is observed below the deposited film (Figure 5b). EDX analysis and the electron diffraction pattern confirms that the composition of the coating is TiO₂ and corresponds to the anatase phase.

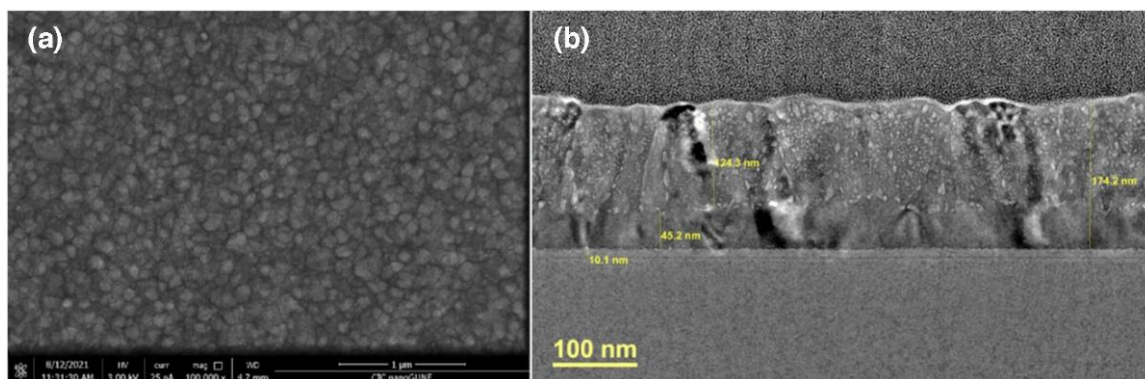


Figure 5. Surface SEM (a) and cross-sectional HRTEM (b) images of a coated-glass fabricated from an inorganic-organic thin film composed of TiO₂ layers (prepared by TiCl₄/H₂O ALD) and hybrid Ti/HQ layers (prepared by TiCl₄/HQ MLD) (2:8 pulse sequence) after annealing under optimized conditions.

The highly porous TiO₂ anatase layer on top of the coating accounts for the observed photocatalytic activity. However, the appearance of a dense non-porous TiO₂ layer at the bottom of the coating was completely unexpected. We have fabricated a coated-glass under the same deposition conditions increasing the time at maximum temperature (400 °C) in the thermal treatment from 3 to 5 h. The UV-Vis spectra of both coated-glasses showed a strong absorption at 312 nm in the UV region which is attributed to the presence of TiO₂. The estimated bandgaps values using the Tauc method were 3.35 and 3.39 eV, respectively, which are in the expected range for photocatalytic coatings (Figure S21). The spectra also

showed a second absorption band around 368 nm. As the intensity of this absorption is lower in the second sample, it could be tentatively attributed to incomplete removal of the hydroquinone template. However, this coated glass showed significantly lower photocatalytic activity (Figure S14) which might be related to the collapse of the porous structure. Since the deposition conditions did not change throughout the different cycles, we hypothesized that this dense layer was formed during the annealing process.

4. Conclusions

We have developed a convenient ALD/MLD methodology for the deposition of porous TiO₂-coatings on soda-lime glass that show activity in the photocatalytic oxidation of nitrogen oxide. Initially, we studied the deposition of hybrid inorganic-organic coatings using TiCl₄ and EG by MLD, which leads to a maximum NO removal of 4% over 4 h. A study of the annealing process on these samples reveals that long thermal treatments result in the loss of catalytic activity, likely due to the collapse of the porous structure. Subsequently, we explored the preparation of TiO₂-coatings by the deposition of inorganic-organic superlattice thin films. The best performing coating was prepared by deposition of a TiO₂ layer by pulsing TiCl₄/H₂O (2 cycles), followed by hybrid film using TiCl₄ and HQ (8 cycles), repeating this sequence 120 times. The resulting material was able to reduce the NO concentration ca. 15% in three successive photocatalytic cycles of 5 h each. The TEM and SEM images of this TiO₂-coating show two regions, a porous columnar structure on top, and a denser region immediately over the thin layer of SiO₂ deposited by PVD. EDX analysis, nanocrystal electron diffraction and Raman spectroscopy confirm the presence of the anatase phase, which, together with the porosity of the material, accounts for the observed photocatalytic activity.

Supplementary Materials: The following supporting information can be downloaded at: <https://www.mdpi.com/article/10.3390/coatings12040488/s1>. Tables S1–S14: MLD and ALD/MLD thin film deposition and annealing conditions. Figures S1–S14: In-flow monitoring of the photocatalytic degradation of NO(g) by coated-glasses fabricated by MLD and ALD/MLD strategies. Figure S15: Photograph of the experimental setup. Figures S16–S19: Raman spectra of selected coated-glasses. Figure S20: XRD pattern, Figure S21: UV-Vis spectra, and Figures S22–S28: SEM and HRTEM images, of coated-glasses fabricated by a combined ALD/MLD deposition strategy.

Author Contributions: Photocatalytic experimental setup, A.G. and M.I.; methodology, R.A., M.B. and C.M.; writing—original draft preparation, R.A., M.B., M.I. and J.J.P.-T.; writing—review and editing, M.I., C.M. and J.J.P.-T.; funding acquisition, A.G., M.I. and J.J.P.-T. All authors have read and agreed to the published version of the manuscript.

Funding: This research was funded by the Spanish Ministerio de Ciencia e Innovación under the project RTC-2017-6504-5 (MCIU/AEI/FEDER, UE).

Institutional Review Board Statement: Not applicable.

Informed Consent Statement: Not applicable.

Data Availability Statement: Not applicable.

Acknowledgments: The authors gratefully acknowledge the continued support from the company Ariño Duglass. We gratefully acknowledge the helpful discussions with Eugenio Vispe, Chromatography and Spectroscopy Service of the ISQCH, and Dra. Concepción Sánchez, X-ray Diffraction and Fluorescence Analysis Service of the Universidad of Zaragoza.

Conflicts of Interest: The authors declare no conflict of interest.

References

1. Seinfeld, J.H.; Pandis, S.N. *Atmospheric Chemistry and Physics: From Air Pollution to Climate Change*; Wiley: New York, NY, USA, 1998.
2. Brimblecombe, P. *The Effects of Air Pollution on the Built Environment*; Imperial College Press: Cambridge, UK, 2003.
3. Harrison, R.M.; Hester, R.E. *Air Quality in Urban Environments*; Royal Society of Chemistry: Cambridge, UK, 2009.

4. Guo, Q.; Zhou, C.; Ma, Z.; Yang, X. Fundamentals of TiO₂ Photocatalysis: Concepts, Mechanisms, and Challenges. *Adv. Mater.* **2019**, *31*, 1901997. [[CrossRef](#)] [[PubMed](#)]
5. Schneider, J.; Matsuoka, M.; Takeuchi, M.; Zhang, J.; Horiuchi, Y.; Anpo, M.; Bahnemann, D.W. Understanding TiO₂ Photocatalysis: Mechanisms and Materials. *Chem. Rev.* **2014**, *114*, 9919–9986. [[CrossRef](#)] [[PubMed](#)]
6. Nakata, K.; Fujishima, A. TiO₂ photocatalysis: Design and applications. *J. Photochem. Photobiol. C Photochem. Rev.* **2012**, *13*, 169–189. [[CrossRef](#)]
7. Fujishima, A.; Rao, T.N.; Tryk, D.A. Titanium dioxide photocatalysis. *J. Photochem. Photobiol. C Photochem. Rev.* **2000**, *1*, 1–21. [[CrossRef](#)]
8. Fujishima, A.; Zhang, X. Titanium dioxide photocatalysis: Present situation and future approaches. *Chimie* **2006**, *9*, 750–760. [[CrossRef](#)]
9. Lasek, J.; Yu, Y.-H.; Wu, J.C.S. Removal of NO_x by photocatalytic processes. *J. Photochem. Photobiol. C Photochem. Rev.* **2013**, *14*, 29–52. [[CrossRef](#)]
10. Dambournet, D.; Belharouak, I.; Amine, K. Tailored Preparation Methods of TiO₂ Anatase, Rutile, Brookite: Mechanism of Formation and Electrochemical Properties. *Chem. Mater.* **2010**, *22*, 1173–1179. [[CrossRef](#)]
11. Nosheen, S.; Galasso, F.S.; Suib, S.L. Role of Ti–O Bonds in Phase Transitions of TiO₂. *Langmuir* **2009**, *25*, 7623–7630. [[CrossRef](#)]
12. Feist, T.P.; Davies, P.K. The soft chemical synthesis of TiO₂ (B) from layered titanates. *J. Solid State Chem.* **1992**, *101*, 275–295. [[CrossRef](#)]
13. Zhang, J.; Li, M.; Feng, Z.; Chen, J.; Li, C. UV Raman Spectroscopic Study on TiO₂. I. Phase Transformation at the Surface and in the Bulk. *J. Phys. Chem. B* **2006**, *110*, 927–935. [[CrossRef](#)]
14. Su, W.; Zhang, J.; Feng, Z.; Chen, T.; Ying, P.; Li, C. Surface Phases of TiO₂ Nanoparticles Studied by UV Raman Spectroscopy and FT-IR Spectroscopy. *J. Phys. Chem. C* **2008**, *112*, 7710–7716. [[CrossRef](#)]
15. Shi, J.; Chen, J.; Feng, Z.; Chen, T.; Lian, Y.; Wang, X.; Li, C. Photoluminescence Characteristics of TiO₂ and Their Relationship to the Photoassisted Reaction of Water/Methanol Mixture. *J. Phys. Chem. C* **2007**, *111*, 693–699. [[CrossRef](#)]
16. Zhang, J.; Xu, Q.; Li, M.; Feng, Z.; Li, C. UV Raman Spectroscopic Study on TiO₂. II. Effect of Nanoparticle Size on the Outer/Inner Phase Transformations. *J. Phys. Chem. C* **2009**, *113*, 1698–1704. [[CrossRef](#)]
17. Zhang, H.; Banfield, J.F. Understanding Polymorphic Phase Transformation Behavior during Growth of Nanocrystalline Aggregates: Insights from TiO₂. *J. Phys. Chem. B* **2000**, *104*, 3481–3487. [[CrossRef](#)]
18. Ranade, M.R.; Navrotsky, A.; Zhang, H.Z.; Banfield, J.F.; Elder, S.H.; Zaban, A.; Borse, P.H.; Kulkarni, S.K.; Doran, G.S.; Whitfield, H.J. Energetics of nanocrystalline TiO₂. *Colloquium* **2002**, *99*, 6476–6481.
19. Zhang, H.; Chen, B.; Banfield, J.F. The size dependence of the surface free energy of titania nanocrystals. *Phys. Chem. Chem. Phys.* **2009**, *11*, 2553–2558. [[CrossRef](#)]
20. Ding, X.-Z.; Liu, X.-H. Correlation Between Anatase-to-rutile Transformation and Grain Growth in Nanocrystalline Titania Powders. *J. Mater. Res.* **1998**, *13*, 2556–2559. [[CrossRef](#)]
21. Isley, S.L.; Penn, R.L. Relative Brookite and Anatase Content in Sol-Gel Synthesized Titanium Dioxide Nanoparticles. *J. Phys. Chem. B* **2006**, *110*, 15134–15139. [[CrossRef](#)]
22. Ferreira-Neto, E.P.; Ullah, S.; Martinez, V.P.; Yabarrena, J.M.S.C.; Simões, M.B.; Perissinoto, A.P.; Wender, H.; de Vicente, F.S.; Noeske, P.-L.M.; Ribeiro, S.J.L.; et al. Thermally stable SiO₂@TiO₂ Core@shell nanoparticles for application in photocatalytic self-cleaning ceramic tiles. *Mater. Adv.* **2021**, *2*, 2085–2096. [[CrossRef](#)]
23. Ma, Y.; Wang, X.; Jia, Y.; Chen, X.; Han, H.; Li, C. Titanium Dioxide-Based Nanomaterials for Photocatalytic Fuel Generations. *Chem. Rev.* **2014**, *114*, 9987–10043. [[CrossRef](#)]
24. Wang, Y.; Li, B.; Zhang, C.; Cui, L.; Kang, S.; Li, X.; Zhou, L. Ordered mesoporous CeO₂-TiO₂ composites: Highly efficient photocatalysts for the reduction of CO₂ with H₂O under simulated solar irradiation. *Appl. Catal. B* **2013**, *130–131*, 277–284. [[CrossRef](#)]
25. Carp, O.; Huisman, C.L.; Reller, A. Photoinduced reactivity of titanium dioxide. *Prog. Solid State Chem.* **2004**, *32*, 33–177. [[CrossRef](#)]
26. Pham, K.; Pelisset, S.; Kinnunen, N.; Karvinen, P.; Hakala, T.K.; Saarinen, J.J. Controlled photocatalytic activity of TiO₂ inverse opal structures with atomic layer deposited (ALD) metal oxide thin films. *Mater. Chem. Phys.* **2022**, *277*, 125533. [[CrossRef](#)]
27. Chen, M.; Chu, J.-W. NO_x photocatalytic degradation on active concrete road surface—From experiment to real-scale application. *J. Clean. Prod.* **2011**, *19*, 1266–1272. [[CrossRef](#)]
28. Hu, Y.; Higashimoto, S.; Martra, G.; Zhang, J.; Matsuoka, M.; Coluccia, S.; Anpo, M. Local Structures of Active Sites on Ti-MCM-41 and Their Photocatalytic Reactivity for the Decomposition of NO. *Catal. Lett.* **2003**, *90*, 161–163. [[CrossRef](#)]
29. Zheng, Z.; Huang, B.; Qin, X.; Zhang, X.; Dai, Y. Strategic Synthesis of Hierarchical TiO₂ Microspheres with Enhanced Photocatalytic Activity. *Chem. Eur. J.* **2010**, *16*, 11266–11270. [[CrossRef](#)] [[PubMed](#)]
30. Liu, B.; Nakata, K.; Sakai, M.; Saito, H.; Ochiai, T.; Murakami, T.; Takagi, K.; Fujishima, A. Mesoporous TiO₂ Core-Shell Spheres Composed of Nanocrystals with Exposed High-Energy Facets: Facile Synthesis and Formation Mechanism. *Langmuir* **2011**, *27*, 8500–8508. [[CrossRef](#)]
31. Li, H.; Bian, Z.; Zhu, J.; Zhang, D.; Li, G.; Huo, Y.; Li, H.; Lu, Y. Mesoporous Titania Spheres with Tunable Chamber Structure and Enhanced Photocatalytic Activity. *J. Am. Chem. Soc.* **2007**, *129*, 8406–8407. [[CrossRef](#)]

32. Chen, Y.; Tian, G.; Ren, Z.; Tian, C.; Pan, K.; Zhou, W.; Fu, H. Solvothermal Synthesis, Characterization, and Formation Mechanism of a Single-Layer Anatase TiO₂ Nanosheet with a Porous Structure. *Eur. J. Inorg. Chem.* **2011**, 754–760. [[CrossRef](#)]
33. Zhan, S.; Chen, D.; Jiao, X.; Tao, C. Long TiO₂ Hollow Fibers with Mesoporous Walls: Sol–Gel Combined Electrospun Fabrication and Photocatalytic Properties. *J. Phys. Chem. B* **2006**, *110*, 11199–11204. [[CrossRef](#)]
34. Ponnusamy, D.; Madanagurusamy, S. Porous Anatase TiO₂ Thin Films for NH₃ Vapour Sensing. *J. Electron. Mater.* **2015**, *44*, 4726–4733. [[CrossRef](#)]
35. Sanzaro, S.; Smecca, E.; Mannino, G.; Bongiorno, C.; Pellegrino, G.; Neri, F.; Malandrino, G.; Catalano, M.R.; Condorelli, G.G.; Iacobellis, R.; et al. Multi-Scale-Porosity TiO₂ scaffolds grown by innovative sputtering methods for high throughput hybrid photovoltaics. *Sci. Rep.* **2016**, *6*, 39509. [[CrossRef](#)] [[PubMed](#)]
36. Garcia-Valenzuela, A.; Alvarez, R.; Rico, V.; Cotrino, J.; Gonzalez-Elipe, A.R.; Palmero, A. Growth of nanocolumnar porous TiO₂ thin films by magnetron sputtering using particle collimators. *Surf. Coat. Technol.* **2018**, *343*, 172–177. [[CrossRef](#)]
37. Arconada, N.; Durán, A.; Suárez, S.; Portela, R.; Coronado, J.M.; Sánchez, B.; Castro, Y. Synthesis and photocatalytic properties of dense and porous TiO₂-anatase thin films prepared by sol–gel. *Appl. Catal. B Environ.* **2009**, *86*, 1–7. [[CrossRef](#)]
38. Abdulagatov, A.I.; Hall, R.A.; Sutherland, J.L.; Lee, B.H.; Cavanagh, A.S.; George, S.M. Molecular Layer Deposition of Titanicene Films using TiCl₄ and Ethylene Glycol or Glycerol: Growth and Properties. *Chem. Mater.* **2012**, *24*, 2854–2863. [[CrossRef](#)]
39. Ishchuk, S.; Taffa, D.H.; Hazut, O.; Kaynan, N.; Yerushalmi, R. Transformation of Organic–Inorganic Hybrid Films Obtained by Molecular Layer Deposition to Photocatalytic Layers with Enhanced Activity. *ACS Nano* **2012**, *6*, 7263–7269. [[CrossRef](#)]
40. Sarkar, D.; Ishchuk, S.; Taffa, D.H.; Kaynan, N.; Berke, B.A.; Bendikov, T.; Yerushalmi, R. Oxygen-Deficient Titania with Adjustable Band Positions and Defects; Molecular Layer Deposition of Hybrid Organic–Inorganic Thin Films as Precursors for Enhanced Photocatalysis. *J. Phys. Chem. C* **2016**, *120*, 3853–3862. [[CrossRef](#)]
41. George, S.M.; Lee, B.H.; Yoon, B.; Abdulagatov, A.I.; Hall, R.A. Metalcones: Hybrid Organic-Inorganic Films Fabricated Using Atomic and Molecular Layer Deposition Techniques. *J. Nanosci. Nanotechnol.* **2011**, *11*, 7948–7955. [[CrossRef](#)]
42. Liang, X.; Yu, M.; Li, J.; Jiang, Y.-B.; Weimer, A.W. Ultra-thin microporous mesoporous metal oxide films prepared by molecular layer deposition (MLD). *Chem. Commun.* **2009**, *46*, 7140–7142. [[CrossRef](#)]
43. Chen, C.-Q.; Li, P.; Wang, G.-Z.; Yu, Y.; Duan, F.-F.; Chen, C.-Y.; Song, W.-G.; Qin, Y.; Knez, M. Nanoporous Nitrogen-Doped Titanium Dioxide with Excellent Photocatalytic Activity under Visible Light Irradiation Produced by Molecular Layer Deposition. *Angew. Chem. Int. Ed.* **2013**, *52*, 9196–9200. [[CrossRef](#)]
44. Dey, N.K.; Kim, M.J.; Kim, K.-D.; Seo, H.O.; Kim, D.; Kim, Y.D.; Lim, D.C.; Lee, K.H. Adsorption and photocatalytic degradation of methylene blue over TiO₂ films on carbon fiber prepared by atomic layer deposition. *J. Mol. Catal. A Chem.* **2011**, *337*, 33–38. [[CrossRef](#)]
45. Kim, S.; Chang, H.-K.; Kim, K.B.; Kim, H.-J.; Lee, H.-N.; Park, T.J.; Park, Y.M. Highly Porous SnO₂/TiO₂ Heterojunction Thin-Film Photocatalyst Using Gas-Flow Thermal Evaporation and Atomic Layer Deposition. *Catalysts* **2021**, *11*, 1144. [[CrossRef](#)]
46. Buchalska, M.; Surówka, M.; Hämäläinen, J.; Iivonen, T.; Leskelä, M.; Macyk, W. Photocatalytic activity of TiO₂ films on Si support prepared by atomic layer deposition. *Catal. Today* **2015**, *252*, 14–19. [[CrossRef](#)]
47. Russell, H.S.; Frederickson, L.B.; Hertel, O.; Ellermann, T.; Jensen, S.S. A Review of Photocatalytic Materials for Urban NO_x Remediation. *Catalysts* **2021**, *11*, 675. [[CrossRef](#)]
48. ISO 22197-1:2007; Fine Ceramics, Advanced Technical Ceramics—Test Method for Air-Purification Performance of Semiconducting Photocatalytic Materials. Part 1: Removal of Nitric Oxide. International Organization for Standardization: Geneva, Switzerland, 2007; Note that ISO 22197-1:2007 has been updated by ISO 22197-1:2016.
49. Devahasdin, S.; Fan, C., Jr.; Li, K.; Chen, D.H. TiO₂ photocatalytic oxidation of nitric oxide: Transient behavior and reaction kinetics. *J. Photochem. Photobiol. A Chem.* **2003**, *156*, 161–170. [[CrossRef](#)]
50. Mills, A.; Elouali, S. The nitric oxide ISO photocatalytic reactor system: Measurement of NO_x removal activity and capacity. *J. Photochem. Photobiol. A Chem.* **2015**, *305*, 29–36. [[CrossRef](#)]
51. Baptista, A.; Silva, F.; Porteiro, J.; Míguez, J.; Pinto, G. Sputtering Physical Vapour Deposition (PVD) Coatings: A Critical Review on Process Improvement and Market Trend Demands. *Coatings* **2018**, *8*, 402. [[CrossRef](#)]
52. Guanghui, F.; Jiafeng, D.; Donghui, P.; Ouli, H. The migration of alkali ions from glass substrates coated with sol-gel barrier films. *J. Non-Cryst. Solids* **1989**, *112*, 454–457. [[CrossRef](#)]
53. Ullah, S.; Ferreira-Neto, E.P.; Pasa, A.A.; Alcantara, C.C.J.; Acuña, J.J.S.; Bilmes, S.A.; Martínez Ricci, M.L.; Landers, R.; Zampieri Fermino, T.; Rodrigues-Filho, U.P. Enhanced photocatalytic properties of core@shell SiO₂@TiO₂ nanoparticles. *Appl. Catal. B* **2015**, *179*, 333–343. [[CrossRef](#)]
54. Niemälä, J.-P.; Karppinen, M. Tunable optical properties of hybrid inorganic-organic [(TiO₂)_m(Ti-O-C₆H₄-O)_k]_n superlattice thin films. *Dalton Trans.* **2015**, *44*, 591–597. [[CrossRef](#)]
55. Schaffer, M.; Schaffer, B.; Ramasse, Q. Sample preparation of atomic-resolution STEM at low voltages by FIB. *Ultramicroscopy* **2012**, *114*, 62–71. [[CrossRef](#)] [[PubMed](#)]
56. Makuła, P.; Pacia, M.; Macyk, W. How to correctly determine the band gap energy of modified semiconductor photocatalysts based on UV–Vis spectra. *J. Phys. Chem. Lett.* **2018**, *9*, 6814–6817. [[CrossRef](#)] [[PubMed](#)]
57. Klepper, K.B.; Nilsen, O.; Fjellvag, H. Deposition of thin films of organic-inorganic hybrid materials based on aromatic carboxylic acids by atomic layer deposition. *Dalton Trans.* **2010**, *39*, 11628–11635. [[CrossRef](#)] [[PubMed](#)]

-
58. Klepper, K.B.; Nilsen, O.; Hansen, P.-A.; Fjellvag, H. Atomic layer deposition of organic-inorganic hybrid materials based on saturated linear carboxylic acids. *Dalton Trans.* **2011**, *40*, 4636–4646. [[CrossRef](#)]
 59. Yang, F.; Brede, J.; Ablat, H.; Abadia, M.; Zhang, L.; Rogero, C.; Elliot, S.D.; Knez, M. Reversible and Irreversible Reactions of Trimethylaluminum with Common Organic Functional Groups as a Model for Molecular Layer Deposition and Vapor Phase Infiltration. *Adv. Mater. Interfaces* **2017**, *4*, 1700237. [[CrossRef](#)]